Article

Off-Planar Geometry and Structural Instability of EDO-TTF Explained by Using the Extended Debye Polarizability Model for Bond Angles

Gerrit-Jan Linker,*[,†] Piet Th. van Duijnen,[†] Paul H. M. van Loosdrecht,[‡] and Ria Broer[†]

[†]Theoretical Chemistry and [‡]Optical Condensed Matter Physics, Zernike Institute for Advanced Materials, University of Groningen, Nijenborgh 4, 9747 AG Groningen, The Netherlands

Ⓢ Supporting Information

ABSTRACT: The geometry of ethylenedioxy-tetrathiafulvalene, EDO-TTF, plays an important role in the metal−insulator transition in the charge transfer salt $(EDO\text{-}TTF)_2PF_6$. The planar and off-planar geometrical conformations of the EDO-TTF molecules are explained using an extended Debye polarizability model for the bond angle. The geometrical structure of EDO-TTF is dictated by its four sulfur bond angles and these are, in turn, determined by the polarizability of the sulfur atoms. With Hartree−Fock and second-order Møller−Plesset perturbation theory calculations on EDO-TTF, TTF, H_2S, and their oxygen and selenium substituted counterparts we confirm this hypothesis. The Debye polarizability model for bond angles relates directly the optimum bond angle with the polarizability of the center atom. Considering the $(EDO\text{-}TTF)_2PF_6$ material in this light proves to be very fruitful.
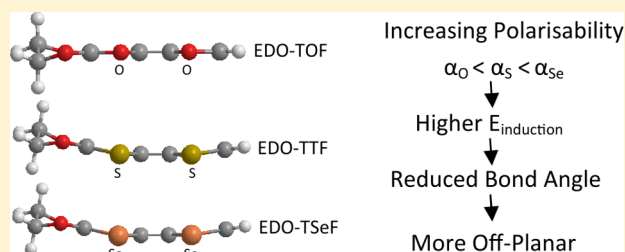
1. INTRODUCTION

Several molecular crystals of EDO-TTF exhibit a metal−insulator transition. In the $(EDO\text{-}TTF)_2PF_6$ charge transfer crystal, this phase transition occurs at 278 K,[1] which can also be induced by light. It is found using X-ray crystallography[2] (Figure 1a,b) that in the high temperature conducting phase
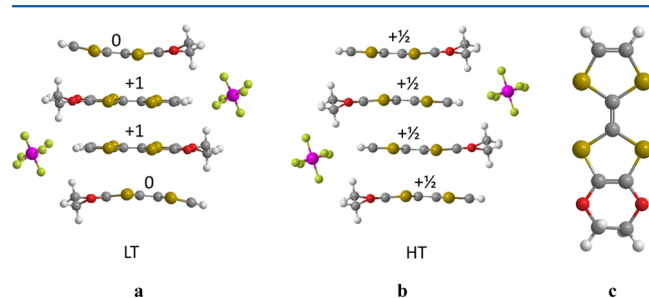

Figure 1. X-ray crystal structures at low temperature (a) and at high temperature (b). The EDO-TTF molecular charge is shown. Top view of the EDO-TTF molecule (c).

EDO-TTF exists with only one molecular conformation. The molecules, which contain four sulfur atoms in the center, have nearly planar geometry (Figure 1c) and they are thought to adopt a charge of $+^1/_2$. Per two molecules an electron is donated to a PF_6 acceptor molecule. These are situated in cavities between the stacks that the EDO-TTF molecules form. In the insulating phase at lower temperature, two conformations of the molecules coexist in the crystal: a planar EDO-TTF molecule, which is assigned a positive charge, and a boat shaped conformer of EDO-TTF, to which a neutral charge is assigned.

In previous work we established the one to one relationship of molecular charge and geometry.[3]

The first-order[2] phase transition is thought to be due to several instabilities[1,4−6] most of which are related to the geometry of the EDO-TTF molecules: geometrical deformation, charge ordering, geometrical ordering, and dimerization. EDO-TTF molecules are very flexible and easy to deform.[3] In the gas phase, the energy difference between a planar and a bent EDO-TTF molecule is only a few millielectronvolts. With the direct relation between charge and geometry, the $|0110\rangle$ charge ordering, which has been detected in the low temperature crystal, is directly coupled to a geometrical ordering of $|BPPB\rangle$ (notation: each of the four characters denote a EDO-TTF molecule, 0 or 1 denote respectively a neutral or +1 charged molecule and P and B denote a planar or boat shaped geometrical conformation). In the conducting phase there is no charge ordering as each molecule is thought to have a charge of $+^1/_2$. The molecules in the crystal at high temperature are equidistant whereas the geometrical ordering in the low temperature crystal leads to a dimerization. The distance between the molecular planes along the stacking vector is smallest for planar molecules in the low temperature phase. Iwano et al. have performed density functional theory (DFT) calculations in which they reproduced the $|0110\rangle$ charge ordering[7,8] and in which they identified an electronic dimer.[9] Such a dimerization, also known as a Peierls instability, can cause a band gap to open.

The insulator to metal phase transition can also be induced by light. Directly after absorbing the photon a coherent phonon is detected, which we think corresponds to the bending mode of the EDO-TTF molecules. Lüer et al. show that a similar phenomenon occurs in 1D chains of tetramethyl-TTF cations and that it leads to the phase transition.[10] The photoinduced phase transition (PIPT) in (EDO-TTF)$_2$PF$_6$ is remarkable for the fact that a very low intensity laser pulse can be used. It is estimated that only one in 500−1500 molecules[5,11] is excited by such a pulse. How such a local event leads to a bulk phase transition is subject of speculation.[5,11−15] One possibility we see is the scenario in which a neutral bent molecule is excited to become planar. The geometry change could affect a neighbor molecule to also change geometry, thereby propagating the effect of the excitation. Therefore, also in the PIPT there could be a relation to the geometry of EDO-TTF molecules.

In previous work we established[3] that as soon as an EDO-TTF molecule becomes positively charged, it adopts a planar conformation and the positive charge is predominantly located on the four sulfur atoms. Therefore, a direct relationship between the positive charge of the sulfur atoms and the geometry of the molecule is suspected. In this work, with Hartree−Fock and second-order Møller−Plesset (MP2) perturbation theory, we will confirm our hypothesis that it is the polarizability of sulfur that determines the geometry of EDO-TTF and that of its parent compound TTF. We will show that there is a delicate balance among the polarizability of sulfur, the θ_{C-S-C} bond angle, and the molecular geometry.

Using the Debye polarizability model[16] and our extension of it, we will demonstrate why the EDO-TTF molecules become planar when charged. In fact, we will demonstrate that, in general, this model gives a direct relationship between the electronic polarizability of the atoms and the bond angle. In the final stages of writing this paper we noticed that Donald et al.[17] used similar expressions in models they termed polarized-ion models. These models were taken from work of Rittner,[18] Hildenbrand,[19] and DeKock et al.[20] In their study on bond angles, bending forces and atomization energies of group-2 and group-12 dihalides, bond angles were reproduced well whereas the calculation of forces and energies was more problematic. The group-12 dihalides proved to be beyond the capabilities of these classical models. The problems were ascribed to electron correlation and relativistic effects. We will show that by using the extended Debye model qualitatively, important general trends for the bond angle can be deduced and that these trends hold very well.

There are alternative models to explain the bond angle, such as the valence shell electron pair repulsion (VSEPR) model.[21] Taking the bond angle in H$_2$O as an example, repulsion arguments are used in this model to explain the angle. All bonds and lone pairs of valence electrons are considered to be mutually repulsive. The angle for H$_2$O forms by a priori assuming sp^3 hybridization so the electron pairs arrange in a tetrahedron with angles of 109.2°. To arrive at the water angle of 104°, the lone pairs are thought to repel more than the electrons in the O−H bonds, allowing the θ_{H-O-H} angle to become sharper. It is commonly assumed that the lone pairs are directed outward from oxygen. Actually, the H$_2$O electron density is not far from spherical, the only distortions are due to the hydrogen atoms that can be seen as drawn into the electron density of oxygen. The small anisotropy of the polarizability is a good indication for the nearly spherical electron density. From accurate CCSD calculations[22] and with the definition for the anisotropy $\zeta = (\alpha_{max} - \alpha_{min})/\bar{\alpha}$, where α_{max} and α_{min}, are respectively the largest and smallest eigenvalues of the polarizability tensor and $\bar{\alpha}$ is the average polarizability, the anisotropy was calculated as 0.094. It is hard to consider the repulsion of the lone pairs when they do not seem to be directed. No a priori assumption of hybridization or arguments about orbital repulsion is needed in the Debye polarizability model. Instead, the observable polarizability of the electron distribution is recognized and, as we will show, induction effects due to it are stabilizing.

The organization of the article is as follows. After a section with computational information we present the Debye polarizability model and our extension of it. The model will be tested using a series of small molecules in section 4. Using our model, the off-planar geometry of TTF will be explained. Next, the geometry of EDO-TTF is discussed by considering the addition of an EDO group to one side of the TTF molecule. The change in geometry is discussed in terms of chemical doping. Before we present our conclusion and discussion, two sections will deal with the transition angle at which the neutral and ionized TTF molecules become off-planar. All geometrical features are discussed in the context of the extended Debye polarizability model and are found to be well explained by it.

2. COMPUTATIONAL INFORMATION

Ab initio calculations are performed to study the effect of induction on the geometry. These calculations are performed at the Hartree−Fock (HF) level of theory (restricted open shell HF for ionized molecules) using the ANO-S basis set.[23] All calculations were performed with the MOLCAS[24] package.

Induction effects relate to perturbing the electron density in response to an electric field; therefore, the wave function needs to be sufficiently flexible. First, the basis set needs to be sufficiently large to allow flexibility to the wave function to describe perturbations. Polarizability is underestimated when smaller basis sets are used, and that leads to reduced induction effects. Second the level at which electron−electron interactions are modeled is an important factor. In HF theory the mean field approximation is used. With MP2 theory, part of the dynamical electron correlation is recovered and this improves the simulation of induction effects considerably. Because we need to model the induction effects and not calculate the polarizabilities themselves, we choose to use the HF level of theory and the ANO-S basis set for the calculations on TTF and EDO-TTF. With this choice we aim to balance accuracy and computational effort. For a detailed study of the geometry of EDO-TTF at the CASSCF and DFT level we refer to our earlier work.[3] The calculations on small molecules are performed at the MP2 level using the RHF/ROHF wave function as reference. The molecules H$_2$Te, H$_2$Po, SbH$_3$, and BiH$_3$ are modeled using the relativistic ANO-RCC basis set. Scalar relativistic effects are taken into account by using the Douglass−Kroll−Hess transformation of the Hamiltonian.[25,26]

The atomic polarizabilities used in the Debye model are taken from the library of the discrete reaction field program: DRF90.[27] Some of these are optimized to reproduce molecular polarizabilities of a series of molecules;[28] others are taken from atomic calculations.

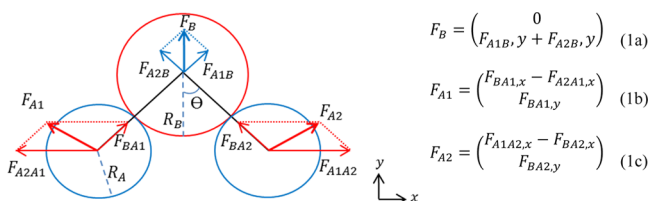**Table 1. Atomic Polarizabilities (/bohr^3) Taken from the DRF90 Library**

atom	α	atom	α	atom	α	atom	α
H	2.79	Cl	16.20	Se	30.77	Po	59.93
F	3.00	S	16.70	As	35.23	Bi	64.59
O	5.75	Br	23.57	Te	49.27		
N	6.56	P	29.83	Sb	54.39		

3. DEBYE POLARIZABILITY MODEL

In 1929 Debye used a simple electrostatic model[16] to make the dipole moment of H_2O and its bent structure plausible. For the general A_2B systems we use the same model and extend it.

In the Debye model the polarizability of electron density is recognized. When molecular polarizability is split, arbitrarily, into atomic parts, a molecule can be viewed as a set of polarizable atoms or ions. These respond to the electric field due to the rest of the molecule. The induced electric moments thus formed have interaction with the field. Debye recognized that in H_2O the induction energy increases with a smaller bond angle, and that it is counteracted by Coulomb repulsion between the two partially charged protons. The present interest is the stability of the general A_2B molecule with respect to changes in the bond angle and to the ratio of the polarizabilities of A and B.

In the model for A_2B we take for A^{+q} and B^{-2q} hard spheres of radius R_A and R_B, respectively, fixing the bond length to $R = R_A + R_B$. We use the classical relation between radius and polarizability of a conducting sphere. This means that the atomic polarizabilities are $\alpha_A = R_A^3$ and $\alpha_B = R_B^3$. With this, we take polarizability to be associated with volume and hence with the bond length R. In contrast, in polarized-ion models this connection is not realized and α and R are used as independent model parameters. Furthermore, the polarizabilities used in these models are for ionized atoms. They are much smaller than those of neutral atoms. Actually, for a qualitative model like ours, it is sufficient to recognize that atoms are polarizable and it is only the ratio of the polarizabilities that is important. The relative energy we calculate depends on the geometry, in which we vary only the bond angle 2θ (Figure 2). Independent variations of the bond length are not allowed in the model.

$$F_B = \begin{pmatrix} 0 \\ F_{A1B, y} + F_{A2B, y} \end{pmatrix} \quad (1a)$$

$$F_{A1} = \begin{pmatrix} F_{BA1, x} - F_{A2A1, x} \\ F_{BA1, y} \end{pmatrix} \quad (1b)$$

$$F_{A2} = \begin{pmatrix} F_{A1A2, x} - F_{BA2, x} \\ F_{BA2, y} \end{pmatrix} \quad (1c)$$

Figure 2. Electric fields and parameters of the model.

Assuming linear response and approximating the polarizability of atom i as a point polarizability α_i, a point dipole moment $\vec{\mu}_i = \alpha_i \vec{F}_i$ is induced at the expense of polarization energy $U_{pol}^i = +^1/_2 \alpha_i F_i^2$. We allow three types of interactions between the atoms in the model. Using i and j as atom labels, the interaction energies are U_{qq}^{ij} for charge−charge interations, U_{qd}^i for the interaction of the induced dipole i with its inducing field, and U_{dd}^{ij} for the dipole−dipole interaction:

$$U_{qq}^{ij} = \frac{q_i q_j}{R_{ij}} \quad (2)$$

$$U_{qd}^i = -\vec{\mu}_i \cdot \vec{F}_i = -\alpha_i F_i^2 \quad (3)$$

$$U_{dd}^{ij} = \frac{-1}{R_{ij}^3}\left(\vec{\mu}_i^\dagger \vec{R}_{ij} \vec{R}_{ij}^\dagger \vec{\mu}_j \frac{3}{R_{ij}^2} - \vec{\mu}_i^\dagger \mathbf{1} \vec{\mu}_j \right) \quad (4)$$

Note that in the expression for U_{dd}, $\mathbf{1}$ represents the unit matrix.

With the polarization energy and the interaction energies we can build the models. First, the original Debye model will be presented where a dipole is induced only on the central atom. Next, we will extend the model to allow induction on all three centers and in which we allow all interactions.

3.1. Original Debye Polarizability Model. By only considering induction on oxygen in H_2O, Debye made its bent structure plausible. We arrive at the Debye polarizability model by setting $\alpha_A = 0$. Hence R becomes equal to R_B, thereby reducing atoms A to point charges. The electric field at B is $F_{B,x} = 0$; $F_{B,y} = (2q \cos \theta)/R^2$. Using eqs 1a and eqs 2−4, the total energy U_{Debye} becomes

$$
\begin{aligned}
U_{Debye} &= U_{qq}^{BA1} + U_{qq}^{BA2} + U_{qq}^{A1A2} + U_{pol}^B + U_{qd}^B \\
&= \frac{q^2}{R}\left(\frac{1}{2 \sin \theta} - 4 - \frac{2\alpha_B \cos^2 \theta}{R^3} \right)
\end{aligned} \quad (5)
$$

To find the extremes, we differentiate the total energy with respect to θ:

$$
\begin{aligned}
\frac{\partial U_{Debye}}{\partial \theta} &= \frac{q^2}{R}\left[\frac{-\cos \theta}{2 \sin^2 \theta} + \frac{4\alpha_B \cos \theta \sin \theta}{R^3} \right] \\
&= \frac{-q^2}{R} \cos \theta \left[\frac{1}{2 \sin^2 \theta} - \frac{4\alpha_B \sin \theta}{R^3} \right]
\end{aligned} \quad (6)
$$

Requiring $\partial U_{Debye}/\partial \theta = 0$ gives for the minimum

$$\left[\frac{1}{2 \sin^2 \theta} - \frac{4\alpha_B \sin \theta}{R^3} \right] = 0 \rightarrow \sin^3 \theta = \frac{1}{8\frac{\alpha_B}{R^3}} = \frac{1}{8} \quad (7)$$

A plot of the energy vs the angle in Figure 3 shows clearly the repulsion of the A^{+q} ions dominate at small angles. At large angles the induction energy is small because the resulting field at B vanishes and in U_{qq} the repulsion is dominant. The linear structure corresponds to a maximum. From eq 7 it follows that the minimum in the original Debye model is at $\theta = 30°$, which corresponds to a bond angle $2\theta = 60°$.

3.2. Extended Debye Polarizability Model. Extending the Debye polarizability model to include induction on all atoms of A_2B, the finite size of the A atoms needs to be recognized: $\alpha_A > 0$ and $R = \alpha_A^{3/2} + \alpha_B^{3/2}$. For convenience we take $\alpha_B = 1$ and $\alpha_A = \beta$. The first consequence of the finite size of the A atoms is that there is a minimum angle: $\sin \theta_{min} = \beta^{3/2}/(1 + \beta^{3/2})$ (Figure 5), where the minimum bond angle (dashed line) $2\theta_{min}$ is plotted against β. Besides the electric field on atom B also the field on atoms A1 and A2 now play a role. For eqs 1a−c we write
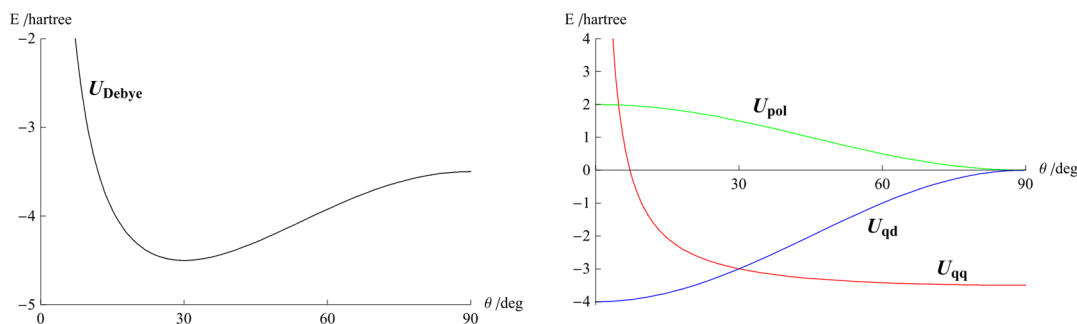
Figure 3. Energy vs angle θ for U_{Debye} (left) and its components (right).
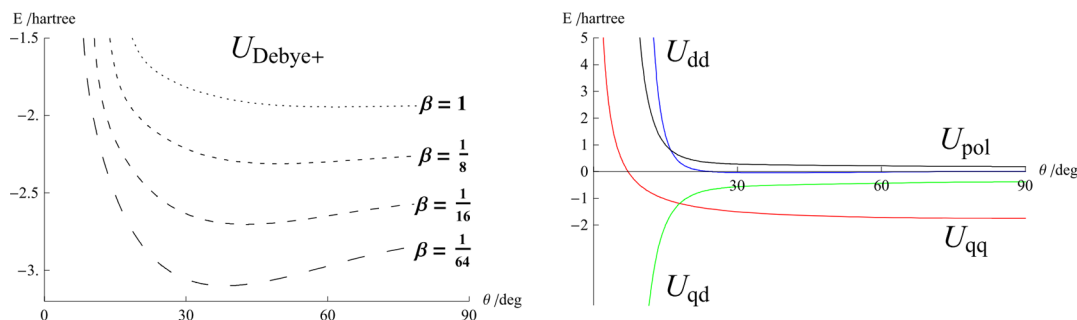

Figure 4. $U_{\text{Debye+}}$ (left) and its components (right; $\beta = 1$) as a function of θ.

$$F_{A1} = \frac{q}{R^2}\begin{pmatrix} 2\sin\theta - \dfrac{1}{4\sin^2\theta} \\ 2\cos\theta \end{pmatrix} \tag{8}$$

$$F_{A2} = \begin{pmatrix} -F_{A1,x} \\ F_{A1,y} \end{pmatrix} \tag{9}$$

$$F_B = \frac{q}{R^2}\begin{pmatrix} 0 \\ 2\cos\theta \end{pmatrix} \tag{10}$$

With these electric fields (eqs 8−10), the total energy $U_{\text{Debye+}}$ can be calculated as

$$U_{\text{Debye+}} = U_{qq} + U_{\text{pol}} + U_{qd} + U_{dd} \tag{11}$$

in which all energy terms have contributions from all three atoms. Recognizing that the induction energy at atom i is $U_{\text{ind}}^i = U_{\text{pol}}^i + U_{qd}^i = -\frac{1}{2}\alpha_i F_i^2$ we get

$$U_{\text{Debye+}} = U_{qq} + U_{\text{ind}} + U_{dd} \tag{12}$$

with

$$U_{qq} = \frac{q^2}{R}\left(-4 + \frac{1}{2\sin\theta}\right) \tag{13}$$

$$U_{\text{ind}} = \frac{-2q^2}{R^4}\left(\cos^2\theta + 2\beta - \frac{\beta}{2\sin\theta} + \frac{\beta}{32\sin^4\theta}\right) \tag{14}$$

$$U_{dd} = \frac{q^2\beta^2}{R^7}\left(\frac{-16\cos^2\theta}{\beta} + \frac{3\cos\theta}{\beta\tan\theta} + \frac{1}{2\sin\theta} + \frac{1}{2\sin^3\theta} \right.$$
$$\left. - \frac{1}{4\sin^4\theta} + \frac{1}{64\sin^7\theta}\right) \tag{15}$$

Using eqs 13−15 in eq 12 and expressing the total energy in terms of β and θ we get

$$\frac{U_{\text{Debye+}}}{q^2} = \frac{1}{(1 + \sqrt[3]{\beta})}\left(-4 + \frac{1}{2\sin\theta}\right)$$
$$- \frac{2}{(1 + \sqrt[3]{\beta})^4}\left(\cos^2\theta + 2\beta - \frac{\beta}{2\sin\theta} + \frac{\beta}{32\sin^4\theta}\right)$$
$$+ \frac{\beta^2}{(1 + \sqrt[3]{\beta})^7}\left(\frac{-16\cos^2\theta}{\beta} + \frac{3\cos\theta}{\beta\tan\theta} + \frac{1}{2\sin\theta} + \frac{1}{2\sin^3\theta} \right.$$
$$\left. - \frac{1}{4\sin^4\theta} + \frac{1}{64\sin^7\theta}\right) \tag{16}$$

Because this is a qualitative model, we view the partial charges q of the atoms merely as the sources for the electric field. Not the strength of the field but its presence and structure are important. We analyze further using $q = 1$. In Figure 4 the individual contributions and the total energy are plotted as a function of the angle θ.

Around the optimum angle, all interaction terms are stabilizing when $\beta = 1$. Going to smaller angles the total energy rises sharply, mainly due to the dipole−dipole repulsion. It is noted that at angles smaller than θ_{min} no analysis should be performed.

The minimum of the total energy depends on $\beta = \alpha_A/\alpha_B$ (Figure 5). At values of β larger than approximately 2.5 the optimum bond angle is 180°. With smaller values of β the optimum angle decreases. We draw the following conclusions. The bond angle decreases with larger polarizability α_B. With larger polarizability α_A the bond angle increases.

The model can be improved by using the DRF[27] method, in which the many-body polarization is treated self-consistently. Induced moments generate fields that in turn induce moments at other polarizabilities, and so on ad infinitum. Hence, depending on the molecular geometry, effective polarizabilities[27,29] appear which in general differ from the nominal values as used in the extended Debye model. The optimal angles derived with the extended Debye polarizability model therefore
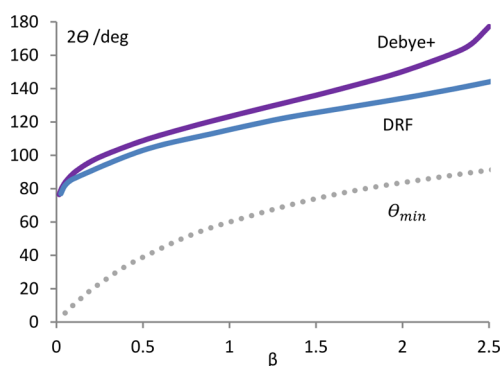
Figure 5. Optimum bond angle (2θ) as a function of β. Dashed line is the minimum bond angle θ_{min}. The two curves represents the extended Debye polarizability model and DRF results.

differ slightly from those derived using the DRF method (see the Debye+ and DRF curves in Figure 5).

Now that we have shown theoretically that the Debye polarizability model can be used to qualitatively predict bond angles, we wish to test its validity by considering the bond angle in a series of small molecules.

4. BOND ANGLES IN SMALL MOLECULES

The dependency of the bond angle on the polarizability will be validated using the following series of molecules: H_2X $X \in \{O, S, Se, Te, Po\}$, XH_3 $X \in \{N, P, As, Sb, Bi\}$, XO_2 $X \in \{N, S, Se\}$, AsX_3 $X \in \{F, Cl, Br,\}$. In all series the polarizability of X increases.

The MP2 bond angles (Figure 6) are all within $1.4°$ of the experimental angles.[30] Angles obtained at the HF level were up to $2°$ larger than those obtained with MP2. The exceptions are SO_2, SeO_2, and AsF_3 which are up to $1°$ smaller and NO_2 which is $4°$ larger. The experimental values for H_2Po, SbH_3, and BiH_3 were not available.

The conclusion from the original Debye polarizability model, that bond angle decreases with increasing polarizability of the central atom, is clearly confirmed in the H_2X and XH_3 series. The prediction of the geometry of H_2O and H_2S is surprisingly accurate. The geometry of NH_3 is also well predicted, and the trend to smaller angles with higher polarizability is observed in the XH_3 series. Note that a larger deviation from $120°$ corresponds to a more pyramidal geometry. The AsX_3 series confirms the additional conclusion drawn from the extended Debye polarizability model: with more polarizable outer atoms the bond angle is larger. These trends, without exceptions, were also found at the HF level in a set of over 140 A_2B molecules

(not shown, information available from the corresponding author).

The series presented here contains molecules with one or two lone pairs on the central atom. All these molecules are nonlinear or pyramidal. When all valence electrons of the central atom are engaged in bonding, the geometry becomes linear or planar. CO_2 is an example of such a linear molecule. Group-13 trihalides, $AlCl_3$, AlF_3, and BF_3, are examples of planar molecules, as are SO_3 and SeO_3. In molecules without nonbonding valence electrons on the central atom, and where at the same time the atom has many electrons in inner shells, these inner electron shells may be sufficiently polarizable to enable a bent geometry. The group-2 hydride BaH_2 is an example of such a molecule.[31]

When all valence electrons participate in bonds, such as in the planar and linear cases above, the polarizability of the central atom is smaller than when there are valence electrons not engaged in bonding. Lower polarizability favors larger bond angles. In addition, the ligands can add or withdraw electrons. For all molecules in the series we examined, electrons are withdrawn from the central atom. SO_3 and SeO_3 illustrate this nicely. The bond angle in SO_2 and SeO_2 is just below $120°$. Adding another oxygen atom removes further electron density from the central atom and the bond angle is increased. SO_3 and SeO_3 are planar molecules.

With the empirical confirmation presented in this section, that the bond angle decreases with higher polarizability of the center atom and that it increases with higher polarizability of the outer atoms, we turn to the discussion of the geometry of TTF whose off−planar geometry can also be understood in these terms.

5. OFF-PLANAR GEOMETRY OF TTF

Now, consider also molecular bending in addition to the bond angle. It is not possible to draw resonant Lewis structures for the neutral TTF molecule. Would such structures exist, delocalization energy could stabilize a planar geometry. In the absence of a stabilizing delocalized π system why should TTF be planar? A boat shape fits best the experimentally observed electron diffraction patterns of TTF in the gas phase.[32] To show that the off-planar molecular geometry of TTF can be attributed to the polarizability of sulfur, the molecular geometry of TTF (tetrathiafulvalene) is compared with that of TOF (tetraoxafulvalene) and TSeF (tetraselenafulvalene). In these molecules the sulfur atoms of TTF are replaced respectively by oxygen atoms (less polarizable) and selenium atoms (more polarizable). The molecular geometry of TOF is planar, TTF is boat shaped and in TSeF the molecular bending is more
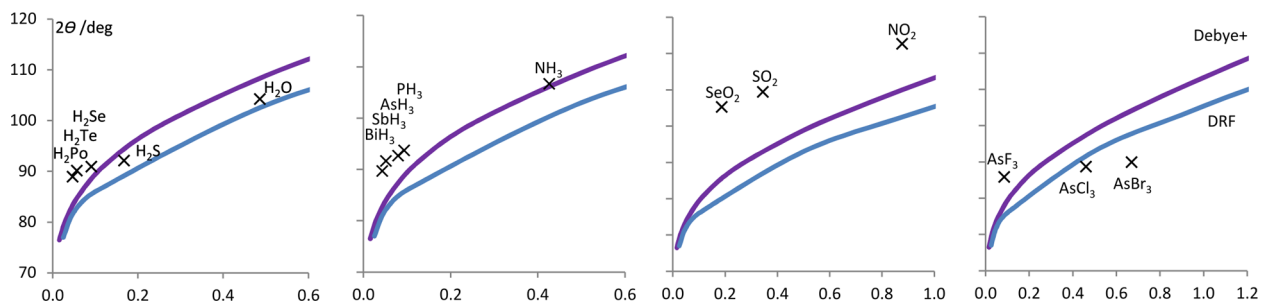

Figure 6. Bond angle 2θ versus β for a series of molecules (see text). The curves of the extended Debye polarizability model and the DRF model are taken from Figure 5. The cross marks indicate the angles we determined from MP2 geometry optimizations.

pronounced. The difference in geometry can be explained in terms of the C—X bond lengths and the θ_{C-X-C} bond angles in the series TXF, where $X \in \{O, S, Se\}$.

In Figure 7 a projection is presented where the three molecules are superimposed such that the four X atoms are in
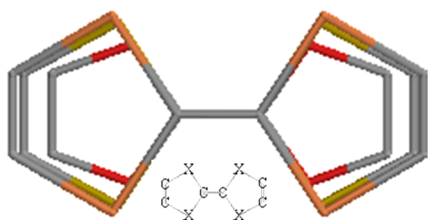

Figure 7. Projection of optimized geometries (omitting H's). From inside to outside: TOF, TTF, and TSeF.

the *xy* plane. Note that the three C=C bonds are almost equal in length (1.30−1.32 Å) and that the main differences are the four C—X bond lengths and the θ_{C-X-C} angles inside each five-ring. The C—O, C—S, and C—Se bond lengths are respectively 1.36, 1.77, and 1.92 Å. The increase of the bond length can be seen as the increase of the size of the X atom, which clearly increases with larger polarizability. Consider a planar five-ring in TXF. Replacing O with S or Se, the bond length is increased and the ring angles adapt. The θ_{C-X-C} angles decrease in the planar TXF series as 105.0°, 95.0°, and 93.5°. Note that these values are close to the equivalent, unconstrained bond angles in H_2O, H_2S, and H_2Se as obtained from HF calculations: 106.2°, 94.1°, and 93.1°, respectively. In the off-planar TTF and TSeF molecules, where the angles are constrained in the five-rings, the θ_{C-X-C} angles are only 0.2° smaller than they are in a planar conformation. Apparently, molecules can lower their energy by adopting smaller θ_{C-X-C} angles and that is only possible when adopting an off-planar geometry. The $\theta_{C-X-X-C}$ dihedral angle, a measure of this off-planarity, becomes 9.2° and 11.1° in TTF and TSeF, respectively. The process that a reduction of too large bond angles in planar rings results in off-planar conformations is well understood. In the text book case of cyclohexane, the θ_{C-C-C} bond angles reduce from 120° in the planar conformation to 112° (value from gas electron diffraction[33] is 111.4°) when adopting the chair conformation, lowering the total HF energy by 1.2 eV.
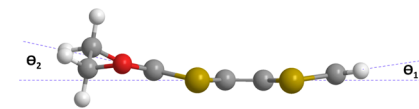
In 1997, Demiralp and Goddard[34] found TTF and TSeF to be planar at the HF level of theory. They concluded that TTF adopts an off-planar geometry only when ring strain is introduced due to steric interactions by replacing the H atoms in TTF by bulky ligands such as F or Cl atoms or by CH_3 groups. We believe that the change in molecular bending can be fully explained by the Debye model. By analysis of the atomic charges, the variations of the θ_{C-S-C} angles can be explained in these molecules. Whether this leads to a change in the off-planar molecular geometry depends on the other angles in the ring. When using the 6-31G** basis set for TTF, as Demiralp and Goddard did, and carefully choosing the start geometry, we did find a boat geometry as the global minimum. When the quality of the basis set is increased by using ANO-S, the polarizability on S and Se becomes better modeled and the optimal bent geometries are easier to find in both TTF and TSeF. MP2 results show an enhanced molecular bending of TTF: $\theta_{C-X-X-C} = 19.4°$ where Hargittai[32] determined it experimentally as 13.5°.

Upon ionization, all TXF$^+$ molecules become planar. The θ_{C-X-C} angles increase by 0.5−0.7°. It follows from charge analysis that the charge hole is predominantly located on the X atoms (about 40% for TOF$^+$, about 80% for TTF$^+$ and TSeF$^+$) thereby reducing its polarizability. This reduction leads to a larger θ_{C-X-C} angle below which a planar ring geometry is favored. The determination of which is the subject of section 7. HF geometry optimizations of TTF and TSeF, in which a chair conformation was used as a starting geometry, always led to boat shaped conformations. Clearly the boat shape is favored. When TTF and TSeF are optimized with the constraint to remain planar, the bond lengths and angles essentially remain the same and the total energy is only a few meV higher. The small geometrical changes and the low energy involved in making the molecules planar show how delicate the balance is. In section 7 we will explore this further in ring strain experiments in which the θ_{C-X-C} angle is varied. Now that we understand the TTF geometry, we first discuss the geometry of EDO-TTF in the next section.

6. MOLECULAR GEOMETRY OF EDO-TTF

The molecular geometry of EDO-TTF is comparable to that of TTF with the difference that the bending in the ring with the attached EDO group is more pronounced. This is due to the electronegative EDO group. Analogous to the experiments in the previous section, EDO-TOF, EDO-TTF, and EDO-TSeF are used to study the effect of polarizability on molecule bending. Molecular bending is determined from the $\theta = \theta_{CXXC}$ dihedral angles within a five-ring, as illustrated in Table 2. The

Table 2. Molecular Bending Angles in EDO-TOF, EDO-TTF, and EDO-TSeF

	EDO-TOF	EDO-TTF	EDO-TSeF
θ_1/deg	0.01	9.47	9.54
θ_2/deg	0.09	13.54	14.22

angle θ_1 in the five-ring without the EDO group becomes larger within the molecular series. Comparing the geometry of EDO-TXF with that of TXF, the molecular bending angle θ_1, the bond lengths and bond angles do not change appreciably.

The result of adding the EDO group is a larger bending angle θ_2 (analyzed below). Moreover, there are other small differences in the geometry of the five-ring. Compared to their equivalents in TXF, the bond lengths are equal within 0.01 Å and the bond angles within 3.3°. The most pronounced change is seen in the θ_{C-X-C} angles, which are reduced from 105.0°, 95.0°, and 93.5° in the TXF series to 103.1°, 93.7°, and 92.5° in EDO-TXF series. For a full table of bond angles and bond lengths of EDO-TXF we refer to the Supporting Information of this paper. The other two angles in this five-ring, θ_{X-C-X} and θ_{C-C-X} become slightly larger (0.2−1.4°) but they do not compensate the reduction of the θ_{C-X-C} angle. A decrease of the sum of the ring angles from 540° is a result, to 538.5° and 538.3°, respectively, in EDO-TTF and EDO-TSeF and this is reflected in the larger bending angle θ_2.

A natural bond order (NBO) charge analysis based on the LoProp partitioning[35] shows that the predominant effect of adding the EDO group is that electrons are transferred from the

doubly bounded carbon atoms of the five-ring to which the EDO ring is attached, to the oxygen atoms of the EDO group. In fact, these oxygens each adopt a charge −0.57 in EDO-TXF. The carbon atoms connected to the oxygen atoms of the EDO group supply approximately an equal amount of charge. The thus created charge hole on the carbon atoms of the five-ring is +0.27. The atomic charge for most of the other atoms in the molecule remains essentially the same.

Analyzing further from the perspective of the θ_{C-X-C} bond angle, the effect of adding the EDO group can be summarized as follows. One carbon atom becomes more positive whereas the charges of the other atoms remain the same. In the light of the Debye polarizability models this extra positive charge is regarded as a decrease in atomic polarizability, which results in a decrease of the θ_{C-X-C} angle. That leads to a smaller sum of angles in the five-ring, which in turn leads to a larger molecular bending angle on the side of the molecule to which the EDO group is attached.

We finish this paragraph on EDO-TTF by discussing the optimum geometry of the neutral and ionized molecule in the context of our polarizability model. The geometries were optimized at the RHF level, UHF for EDO-TTF$^+$, using the 6-31G** basis set and the partial charges were obtained using the LoProp partitioning. We analyze the geometry around sulfur atoms S_1 and S_2 in the two five-membered rings (Table 3).

Table 3. Comparing the Optimized Geometries of Neutral and Ionized EDO-TTF

	EDO-TFF^0	EDOTFF$^+$
$\theta_{C2-S2-C4}$/deg	95.0	95.5
q_{C4}	0.0	0.0
q_{S2}	−0.1	0.1
q_{C2}	0.0	0.0
$\theta_{C1-S1-C3}$/deg	93.7	95.1
q_{C1}	0.0	0.0
q_{S1}	−0.1	0.1
q_{C3}	0.0	0,0
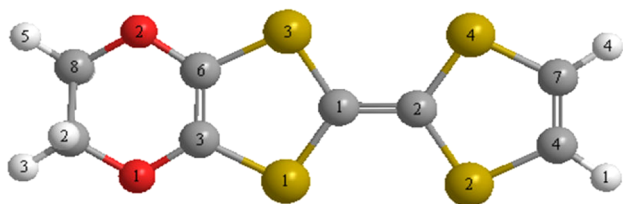
Upon ionization, the θ_{C-S-C} angles increase. This is explained as follows. The charge on the sulfur atoms decreases by 0.2, which we relate to a decrease in atomic polarizability α_S. The charge on the carbon atoms remain almost the same; therefore, α_C remains the same. Hence, the ratio between the polarizabilities, $\beta = \alpha_C/\alpha_S$, is increased and with that our model predicts a larger θ_{C-S-C} angle in the ionized molecule. The sum of the five angles in each ring becomes 540° and hence the molecular geometry becomes planar.

7. DETERMINATION OF THE TRANSITION ANGLE θ_{C-X-C}

The dependence of the molecular bending of neutral TXF on θ_{C-X-C} is determined by varying θ_{X-C-X} and by allowing the remainder of the system to relax in a HF geometry optimization. In setting this angle, ring strain is introduced, which is resolved when the other bonds and angles in the five-ring adjust. In this way the θ_{C-X-C} angle, which determines the molecule bending, can be indirectly tuned. At the point where the molecular geometry becomes off-planar, the sum of the ring angles $\theta_{total} = \theta_{X-C-X} + 2 (\theta_{C-C-X} + \theta_{C-X-C})$ deviates from 540° and a transition angle $\theta_{C-X-C,transition}$ can be determined.

It is observed in Figure 8 that for large θ_{X-C-X} the rings are planar with $\theta_{total} = 540°$. For small values of θ_{X-C-X} the molecules are boat shaped and $\theta_{total} < 540°$. In the planar regime all angles change linearly with θ_{X-C-X}. In the nonplanar regime the change of the θ_{C-X-C} angle is not linear.

The transition angle, at which each molecule becomes bent $(\theta_{C-X-C,transition})$ is 109°, 95°, and 93° in TOF, TTF, and TSeF, respectively. The more polarizable atom X, the smaller the transition angle. The angle θ_{C-X-C} is clearly the weakest bond angle in the ring. When there is room in the ring for a smaller angle θ_{C-X-C} than the transition value, the molecule remains planar. When the other angles in the ring cause the angle θ_{C-X-C} to become larger than the transition value, the geometry of the rings change to nonplanar and θ_{C-X-C} remains close to the value of $\theta_{C-X-C,transition}$.

The procedure is repeated for ionized TXF. As mentioned in section 5, the electron is extracted predominantly from the four X atoms, thereby reducing its atomic polarizability. The expectation from the Debye polarizability model is therefore that θ_{C-X-C} in TXF becomes larger on ionization and that therefore the transition angles should also increase, and this is indeed the case. The transition angles $\theta_{C-X-C,transition}$ found are 123°, 106°, and 102° in TOF$^+$, TTF$^+$, and TSF$^+$, respectively.
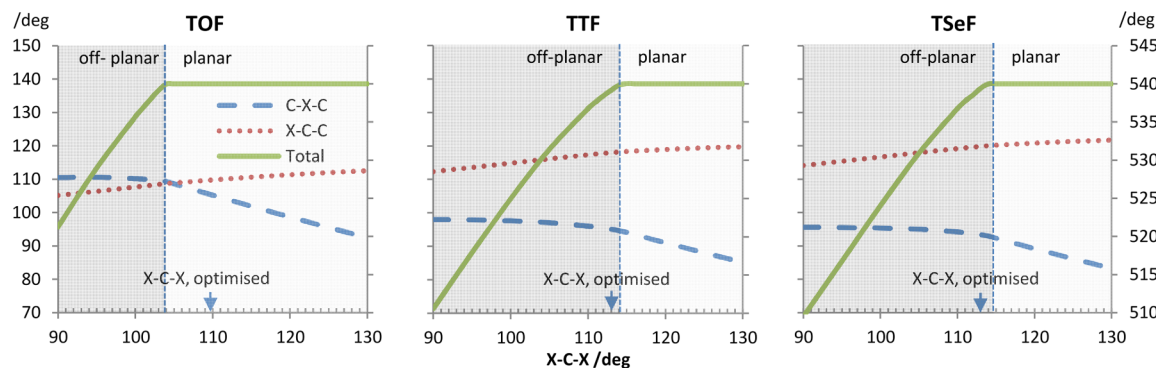

Figure 8. Angles in the five-ring (left axis) and θ_{total} (right axis) with dependence on θ_{X-C-X} (horizontal axis) in TOF, TTF, and TSF. The vertical dashed line separates the planar and off-planar regimes. The arrow indicates θ_{X-C-X} in the fully optimized molecule.

In previous work[3] we have shown that the molecules become planar as soon as they have a positive charge. Whether this also occurs on excitation is a further interesting question. We speculate that upon excitation a bent molecule becomes planar and that this change in geometry can propagate to its neighbor molecule in the TTF stack and form the coherent phonon that is observed at the PIPT. This idea is supported by experiments by Lüer et al.[10] on $(TMTTF^+)_2$ dimers. They found that intermolecular bending and breathing modes are strongly coupled to the electronic transition.

8. CONCLUSIONS

The off-planar molecular geometry of EDO-TTF is explained using the extended Debye polarizability model. The molecular bending originates from the θ_{C-S-C} bond angles. These angles optimize to too small values for the five-rings in the molecule to remain planar. The extended Debye polarizability model gives a direct relation between the polarizability of sulfur and the bond angle. We deduced the following rules: (1) the more polarizable the center atom is, the smaller the bond angle becomes, and (2) the more polarizable the outer atoms are, the larger the bond angle becomes. These relations were confirmed empirically with MP2 theory by optimizing a set of A_2B and A_3B molecules and also by comparing the optimal HF geometry of TTF and EDO-TTF molecules with their selenium and oxygen substituted analogues. The molecules with oxygen substitutes are planar whereas the selenium substitutes have a more pronounced molecular bending.

The more pronounced bending of the ring with the EDO attachment in EDO-TTF is explained as follows. The EDO group withdraws electron density from the carbon atoms to which it is connected, thereby reducing the polarizability of these atoms. This reduces the θ_{C-S-C} angle, which leads to more pronounced off-planar geometry of that five-ring.

It is shown that there is a transition angle $\theta_{C-S-C,\text{transition}}$ at which the TTF molecule becomes off-planar and that this angle depends on the polarizability of S. When S is replaced by O or Se, the angle becomes respectively larger or smaller. Upon ionization of the molecules, the transition angles increase due to the reduced polarizability of the central atom of the bond angle. The larger angle can be accommodated in the planar five-ring; hence, TTF^+ and $EDO\text{-}TTF^+$ are planar.

By elucidating the molecular geometry in this manner, we provide a solid starting point for addressing the questions about the behavior of the bulk material. We feel it is the molecular geometry that may be key in the physics of the system. We recognize that whether or not the molecule is planar is directly coupled to the polarizability of the sulfur atoms. We have shown that a change in bond angle can be related to a change in polarizability which in turn is correlated to a change in partial atomic charge.

ASSOCIATED CONTENT

Ⓢ Supporting Information

Bond angles and bond lengths in the five-rings of EDO-TOF, EDO-TTF, and EDO-TSeF (Table S1). This material is available free of charge via the Internet at http://pubs.acs.org.

AUTHOR INFORMATION

Notes

The authors declare no competing financial interest.

REFERENCES

(1) Saito, K.; Ikeuchi, S.; Ota, A.; Yamochi, H.; Saito, G. *Chem. Phys. Lett.* **2005**, *401*, 76.
(2) Ota, A.; Yamochi, H.; Saito, G. *J. Mater. Chem.* **2002**, *12*, 2600.
(3) Linker, G. J.; van Loosdrecht, P. H. M.; van Duijnen, P.Th.; Broer, R. *Chem. Phys. Lett.* **2010**, *487*, 220−225.
(4) Aoyagi, S.; Kato, K.; Ota, A.; Yamochi, H.; Saito, G.; Suematsu, H.; Sakata, M.; Takata, M. *Ang. Chem. Int. Ed.* **2004**, *43*, 3670−3673.
(5) Yamochi, M.; Koshihara, S. *Sci. Technol. Adv. Mater.* **2009**, *10*, 024305.
(6) Murata, T.; Shao, X.; Nakano, Y.; Yamochi, H.; Uruichi, M.; Yakushi, K.; Saito, G.; Tanaka, K. *Chem. Mater.* **2010**, *22*, 3121−3132.
(7) Iwano, K.; Shimoi, Y. *Phys. Rev. B* **2008**, *77*, 075120.
(8) Iwano, K.; Shimoi, Y. *Phys. Stat. Sol. (c)* **2009**, *1*, 120−123.
(9) Iwano, K.; Shimoi, Y. *J. Phys. Conf. Ser.* **2009**, *148*, 012010.
(10) Lüer, L.; Manzoni, C.; Cerullo, G.; Lanzani, G. *15th International Conference on Ultrafast Phenomena*, 2006; paper ThD26.
(11) Chollet, M.; Guerin, L.; Uchida, N.; Fukaya, S.; Shimoda, H.; Ishikawa, T.; Yamochi, H.; Saito, G.; Tazaki, R.; Adachi, S.; et al. *Science* **2005**, *307*, 86.
(12) Onda, K.; Ishikawa, T.; Chollet, M.; Shao, X.; Yamochi, H.; Saito, G.; Koshihara, S. *J. Phys. Conf. Ser.* **2005**, *21*, 216.
(13) Onda, K.; Ogihara, S.; Ishikawa, T.; Okimoto, Y.; Shao, X. F.; Yamochi, H.; Saito, G.; Koshihara, S. *J. Phys. Condens. Mater.* **2008**, *20*, 224018.
(14) Onda, K.; Ogihara, S.; Ishikawa, T.; Okimoto, Y.; Shao, X. F.; Nakano, Y.; Yamochi, H.; Saito, G.; Koshihara, S. *J. Phys. Conf. Ser.* **2009**, *148*, 012002.
(15) Ogihara, S.; Onda, K.; Shimizu, M.; Ishikawa, T.; Okimoto, Y.; Shao, X. F.; Nakano, Y.; Yamochi, H.; Saito, G.; Koshihara, S. *J. Phys. Conf. Ser.* **2009**, *148*, 012008.
(16) Debye. *Polar Molecules*; Dover: 1929.
(17) Donald, K.; Mulder, W.; Szentpály, L. *J. Chem. Phys.* **2003**, *119*, 5423.
(18) Rittner, E. S. *J. Chem. Phys.* **1951**, *19*, 1030.
(19) Hildenbrand, D. L. *J. Electrochem. Soc.* **1979**, *126*, 1396.
(20) DeKock, R. L.; Peterson, M. A.; Timmer, L. K.; Baerends, E. J.; Vernooijs, P. *Polyhedron* **1990**, *9*, 1919. DeKock, R. L.; Peterson, M. A.; Timmer, L. K.; Baerends, E. J.; Vernooijs, P. Erratum. *Polyhedron* **1991**, *10*, 1965.
(21) Gillespie, R. J.; Matta, C. F. *Chem. Educ. Res. Pract.* **2001**, *2*, 73−90.
(22) Kongsted, J.; Osted, A.; Mikkelsen, K. *J. Chem. Phys.* **2003**, *119*, 1620.
(23) Pierloot, K.; Dumez, B.; Widmark, P. O.; Roos, B. O. *Theor. Chim. Acta* **1995**, *90*, 87.
(24) Karlström, G.; Lindh, R.; Malmqvist, P.; Roos, B. O.; Ryde, U.; Veryazov, V.; Widmark, P.; Cossi, M.; Schimmelpfennig, B.; Neogrady, P.; et al. *Comput. Mater. Sci.* **2003**, *28*, 222.
(25) Douglas, N.; Kroll, N. M. *Ann. Phys.* **1974**, *82*, 89.
(26) Hess, B. A. *Phys. Rev. A* **1986**, *33*, 3742.
(27) Swart, M.; van Duijnen, P. Th. *Mol. Simul.* **2006**, *32*, 471.
(28) van Duijnen, P. Th.; Swart, M. *J. Phys. Chem. A* **1998**, *102* (14), 2399−2407.
(29) Van Duijnen, P. Th.; Swart, M.; Jensen, L. The discrete reaction field approach for calculating solvent effects. In *Solvation Effects on Molecules and Biomolecules: Computational Methods and Applications*; Canuto, S., Ed.; Springer: Berlin, 2008; Vol. 6; p 39.
(30) Lide, D. R. *CRC Handbook of Chemistry and Physics*, 85th ed.; CRC Press: Boca Raton, FL, 2004.
(31) von Szentpály, L *J. Phys. Chem. A* **2002**, *106*, 11945−11949.
(32) Hargittai, I.; Brunvoll, J.; Kolonits, M.; Khodorkovsky, V. *J. Mol. Struct.* **1994**, *317*, 273.

7226

dx.doi.org/10.1021/jp303967s | *J. Phys. Chem. A* 2012, 116, 7219−7227

(33) Bastiansen, O.; Fernholt, L.; Seip, H.; Kambara, H.; Kuchitsu, K. *J. Mol. Struct.* **1973**, *18*, 163−168.

(34) Demiralp, E.; Goddard, W. A., III. *J. Phys. Chem. A* **1997**, *101* (43), 8128−8131.

(35) Gagliardi, L.; Lindh, R.; Karlström, G. *J. Chem. Phys.* **2004**, *121*, 4494.

7227

dx.doi.org/10.1021/jp303967s | *J. Phys. Chem. A* 2012, 116, 7219−7227